LONDON, METEOROLOGICAL OFFICE.
Met.O.15 Internal Report No.77

The role of ice nucleus distributions in cirrus cloud formation: a numerical simulation of the microphysics.

04641088 551.574.11 551.574.13 FH5B

METEOROLOGICAL OFFICE
London Road, Bracknell, Berks.

MET.O.15 INTERNAL REPORT

NUMBER 77

THE ROLE OF ICE NUCLEUS DISTRIBUTIONS IN CIRRUS CLOUD FORMATION: A NUMERICAL SIMULATION OF THE MICROPHYSICS.

by

A.G. Darlison

Met O 15

Cloud Physics Branch (Met.O.15)

THE ROLE OF ICE NUCLEUS DISTRIBUTIONS IN CIRRUS CLOUD FORMATION: A NUMERICAL SIMULATION OF THE MICROPHYSICS

A.G Darlison

Met. O 15

Sept. 1988

ABSTRACT

The aim of this paper is to investigate the nucleation of cirrus cloud by considering the physics of the freezing process and the properties of the aerosol spectrum. This enables us to:

i) Explain why there appear to be several orders of magnitude fewer crystals than nuclei in cirrus,

ii) Predict a dependence of number concentration on updraught velocity,

iii) Explain why crystal number concentrations tend to decrease with temperature,

iv) Interpret observations of liquid water in cirrus and discuss whether there is a shortage of deposition nuclei,

v) Calculate the mean size of initial ice crystals and hence assess instrument response.

These results are summarised by simple parametrizations of the number concentration and peak saturation ratio achieved in terms of updraught velocity and temperature.

1. INTRODUCTION

Cirrus cloud is characterised by the low concentration of ice crystals compared to the number of droplets in most water cloud. Typically, peak concentrations in cirrus are within the range 10^4 to 10^6 m^{-3} (Heymsfield 1975, Varley 1978, Heymsfield and Knollenberg 1972). This is surprising in view of the Fletcher(1962) distribution for ice nuclei (IN),

$$\nu(T) = F \exp(GT_c) \quad (m^{-3}) \qquad (1)$$

where the empirical constants $F = 10^{-2}$ m^{-3} and $G = -0.6^{o}C^{-1}$. This yields $3x10^{8} m^{-3}$ at $-40^{o}C$, for example. This contrasts with the situation in lower cloud where the problem is to explain excess crystal concentrations. Furthermore the Fletcher distribution predicts a rapid increase of crystal concentrations with altitude, which is not observed. For example, Heymsfield and Platt (1983) find a slight decrease. This is borne out by Rangno and Hobbs (1986) who find a peak concentration of about $10^4 m^{-3}$ which does not depend on altitude.

One explanation, suggested by Rangno and Hobbs, is that there is a deficit of IN, relative to the Fletcher distribution, at cirrus levels. When using this distribution we must be aware that it represents observations at temperatures down to about $-30^{o}C$ and extrapolation to lower temperatures may be invalid. A shortage of nuclei acting in the deposition mode is suggested by the following:

i) observations of liquid water at temperatures as low as -36°C (Heymsfield 1977,Sassen 1984),

ii) estimates of the ice water content in aircraft contrails (Bigg and Meade 1971, Knollenberg 1972) which are much greater than the vapour content of the exhaust, suggesting the presence of ice supersaturated but cloud-free layers in the atmosphere,

iii) sea level measurements showning a deficit of deposition nuclei (eg Rosinski et al. 1987).

On the other hand the few direct IN measurements made on samples collected at cirrus levels show an activity spectrum which is not significantly different from (1) (Bigg and Miles 1963, Bigg 1967), although these measurements do not distinguish between nucleation modes, and nor are they made at cirrus temperatures. Even if there were a deficit of deposition nuclei, allowing water saturation to be achieved, we still need to explain why so few droplets freeze, particularly at temperatures below -40°C where homogeneous freezing should be active (Kuhns and Mason 1968). Rangno and Hobbs (1986) also suggest that low crystal counts may be due to poor instrument response to small crystals. Crystals smaller than about 50um would not be counted by their ice detector. A similar limitation applies to PMS optical array probes due to the resolution and response time of the diodes (Brown and Darlison 1988, Baumgardner 1986). A final explanation envisages dilution of the nucleation region by turbulent diffusion and differential sedimentation (Heymsfield and Knollenberg 1972).

The initial ice crystal concentration is an important quantity because it determines the subsequent development of the crystal

spectrum, and hence the radiative and dynamical properties of the cloud. For example low concentrations will result in large crystals with an appreciable fall velocity. It is therefore important to distinguish between the above explanations in order to be able to develop cloud-scale models confidently and also to interpret in-situ microphysics observations.

The condensation of water droplets on hygroscopic nuclei and the subsequent development of the droplet spectrum by condensation and coalescence is reasonably well understood and the theory is capable of reproducing many of the observed features of droplet spectra (Mason 1971 ch3). The aim of this paper is to adopt a similar detailed physical approach to cirrus nucleation and place cirrus microphysics on a sound theoretical footing.

One problem immediately encountered when this approach is adopted is that it is difficult to parametrize the nucleation process due to the great variety of microphysical processes which may be involved. This problem is made worse by a lack of data for nucleus distributions at cirrus levels. In this paper we use three parametrizations, representing three broad classes of nucleation modes. These are of necessity crude and some features have little observational justification. However we are still able to answer many of the above questions because the results of the model turn out to be very insensitive to the details of these parametrizations.

2.THE MODEL

We consider a closed parcel of air undergoing forced ascent with an updraught velocity w. The CCN/droplet spectrum and the ice crystal spectrum are each specified by several size bins. The radius corresponding to each bin is varied explicitly using the growth rate equations (see below). This models the condensation and growth of cloud droplets, and the diffusional growth of ice crystals. The number concentration in each droplet size bin is reduced by freezing processes. Frozen droplets are assigned to adjacent ice crystal size bins. Ice crystal bins are initialised to zero concentrations at the start of a normal model run.

Observations of CCN at cirrus altitude show concentrations similar to those found near sea-level, so we use the model maritime distribution of Junge et al (1971) to determine the initial concentrations in CCN/droplet size bins. We assume that the nuclei are composed of ammonium sulphate. The results below do depend to some extent on what is assumed about the physical properties of the condensation nucleus material, particularly the Van t'Hoft factor (which effects the homogeneous nucleation rate) although we believe our general conclusions to be valid for any realistic assumptions about these.

In the following equations the subscripts S and L denote the solid and liquid phase respectively and P indicates either phase. N denotes nucleus material. Standard notation is adopted and for non-standard symbols the reader is referred to the definitions in Appendix 2.

2.THE MODEL

We consider a closed parcel of air undergoing forced ascent with an updraught velocity w. The CCN/droplet spectrum and the ice crystal spectrum are each specified by several size bins. The radius corresponding to each bin is varied explicitly using the growth rate equations (see below). This models the condensation and growth of cloud droplets, and the diffusional growth of ice crystals. The number concentration in each droplet size bin is reduced by freezing processes. Frozen droplets are assigned to adjacent ice crystal size bins. Ice crystal bins are initialised to zero concentrations at the start of a normal model run.

Observations of CCN at cirrus altitude show concentrations similar to those found near sea-level, so we use the model maritime distribution of Junge et al (1971) to determine the initial concentrations in CCN/droplet size bins. We assume that the nuclei are composed of ammonium sulphate. The results below do depend to some extent on what is assumed about the physical properties of the condensation nucleus material, particularly the Van t'Hoft factor (which effects the homogeneous nucleation rate) although we believe our general conclusions to be valid for any realistic assumptions about these.

In the following equations the subscripts S and L denote the solid and liquid phase respectively and P indicates either phase. N denotes nucleus material. Standard notation is adopted and for non-standard symbols the reader is referred to the definitions in Appendix 2.

Nuclei deliquesce at some critical supersaturation to form haze droplets. Droplet growth rates are given by:

$$r_{Li}\frac{dr_{Li}}{dt} = \frac{\sigma_L - b/T\, r_{Li} + c m_N / r_{Li}^3}{\left\{\frac{L_v \rho_L}{K_a T}\left(\frac{L_v W_L}{RT} - 1\right) + \frac{\rho_L R T}{D W_L e_L^{sat}(T)}\right\}} \qquad (2)$$

(Mason 1971 equation 3.14)

where the thermal conductivity of air and the diffusivity of water vapour in air are given by:

$$K_a = \left(2.382 + 0.00703\, T_c\right) \times 10^{-2} \qquad W m^{-1} K^{-1} \qquad (3)$$

(Beard and Pruppacher 1971)

$$D(p,T) = 2.11 \times 10^{-5}\left(\frac{T}{T_0}\right)^{1.94}\frac{P_0}{P} \qquad m^2 s^{-1} \qquad (4)$$

(Hall and Pruppacher 1976). We are neglecting mean free path effects on D at small radii (Pruppacher and Klett 1978 ch 3). For values of σ_L less than

$$\sigma_{Lc} = \frac{2}{3}\left(\frac{b^3}{3 c m_N T^3}\right)^{1/2} \qquad (5)$$

haze droplets have an equilibrium radius determined by the ambient saturation ratio. It may be found by setting the numerator of (2) to zero and solving for r_i . When σ_L exceeds this value no equilibrium radius exists and haze droplets grow rapidly into mature cloud droplets whose radius is determined by the vapour supply.

Total water is conserved as ascent proceeds so the saturation ratio is given by:

$$d\sigma_p = \frac{-p}{\epsilon e_p^{sat}} \frac{d}{dt}(w_L + w_s) - (1+\sigma_p)\left\{\frac{1}{e_p^{sat}}\frac{de_p^{sat}}{dt} - \frac{w}{p}\frac{dp}{dz}\right\} \quad (6)$$

(Pruppacher and Klett 1978, equation 11). The first term on the right hand side is the reduction in humidity due to condensation. The remaining terms represent the effects of ascent. Mixing ratio is defined in the usual way so;

$$\frac{dw_p}{dt} = \frac{4\pi}{3}\frac{\rho_p}{\rho_a}\left\{\sum_{ip}\frac{dn_{pi}}{dt}r_{pi}^3 + \sum_{ip} r_{pi}^3 n_{pi}\frac{dr_{pi}}{dt}\right\} \quad (7)$$

The temperature of the parcel is determined by conservation of heat

$$\frac{dT}{dt} = -\frac{gw}{c_p} + \frac{L_v}{c_p}\frac{dw_L}{dt} + \frac{L_s}{c_p}\frac{dw_s}{dt} \quad (8)$$

The adiabatic cooling term is usually much larger than the latent heating terms at high altitude, although this may not apply when rapid freezing occurs. Pressure and density are given by the NACA standard atmosphere (Smithsonian Meteorological Tables 1984).

In the absence of ice these equations define a model similar to the early closed-parcel models of cumulus (eg Howell 1949) and we have verified that it gives similar results.

To develop a cirrus microphysics model we include three modes of nucleation:

i) Homogenous nucleation.

The rate of formation of spontaneous nuclei per unit volume is given by the classical formula (Fletcher 1962 p39ff)

$$I(T) = \left\{ \frac{\rho_L kT}{h} \exp(-\Delta g / kT) \right\} \exp(\Delta G^* / kT) \quad (9)$$

where the critical embryo free energy is given by

$$\Delta G^* = \frac{16\pi \varphi_{SL}^3 \xi}{3\{\rho_s kT . \ln(e_L^{sat} / e_s^{sat})\}} \quad (10)$$

The molecular exchange energy Δg is difficult to measure at low temperatures but the constant value $\Delta g = 2.0 \times 10^{-20}$ J seems reasonable (Eadie 1971). Given this value we set the ice-water interfacial free-energy, φ_{SL} so that (9) and (10) reproduce the experimental results of Kuhns and Mason (1968). Assuming the shape factor $\xi = 1$ (spherical embryos) this yields $\varphi_{SL} = 2.4 \times 10^{-2}$ Nm^{-1} which is not inconsistent with Eadies calculation. Note that the final results from the model are not very sensitive to the way we choose Δg and φ_{SL} providing that the combination is consistent with the Kuhns and Mason results.

In addition we must account for the presence of solute. Droplets contain a mole fraction 1-M of solute, where

$$M = \left\{ 1 + J \frac{W_N m_N}{W_L \left(\frac{4\pi}{3} \rho_L r_{Li}^3 - m_N \frac{\rho_L}{\rho_N} \right)} \right\}^{-1} \qquad (11)$$

This inhibits the freezing of haze droplets by reducing the vapour pressure of the liquid phase and its effects are incorporated by multiplying e_L^{sat} by M in (10). For cloud droplets, solute effects are negligible and equations (9) and (10) yield a freezing probability which is proportional to droplet volume and which increases rapidly as temperature falls.

ii) Condensation freezing.

This term is intended to account for all nucleation modes involving the action of an insoluble particle on a droplet. This includes: i) freezing by insoluble particles originally embedded in the hygroscopic nucleus (immersion freezing); ii) insoluble particles which are captured by droplets (contact nucleation); iii) and insoluble particles which act first as condensation nuclei (condensation freezing).

Because of the diverse physical mechanisms operating and a rather poor knowledge of the ice nucleating properties of the cirrus aerosol there is little point in trying to model condensation freezing explicitly. Instead we use a phenomenological model which freezes

droplets at a rate given by

$$\frac{dn_{Li}}{dt} = -\left(n_{Li} V_{Li} \Big/ \sum_j n_{Lj} V_{Lj}\right)\left(\nu(T) - \sum N\right) S_i / \tau_{cf} \quad (12)$$

where $\nu(T)$ is the total number of available ice nuclei, assumed to be given by (1), $\sum N$ is the number of condensation freezing events to date, S_i is a term which suppresses the freezing of haze droplets (as in homogeneous nucleation) and τ_{cf} is a time constant. If we sum this equation over i it gives the rate of change of the total number of droplets. Ignoring the effects of the term S_i this would yield $\nu(T)$ crystals in a characteristic time τ_{cf}. This time constant could in principle be obtained from laboratory measurements of IN in expansion chambers or using filters although little data is available at present. Fortunately the model results are extremely insensitive to this parameter and order of magnitude changes in τ_{cf} result in negligible changes in the number of crystals nucleated. We arbitrarily choose τ_{cf} = 10s. The value of τ_{cf} has been discussed by Gorbunov et al (1987). In practice the final number of crystals is governed mainly by S_i . This falls rapidly when the first crystals to be nucleated start to reduce the humidity faster than ascent increases it. The first term on the right hand side gives droplets a freezing probability proportional to their volume on the grounds that larger droplets are more likely to contain or capture insoluble material.

iii) Deposition nucleation.

Most of the measurements incorporated in the Fletcher distribution are made at water saturation. We assume that a certain fraction f ($0<f<1$) of the nuclei given by (1) are deposition nuclei active at water saturation. At lower ice super-saturations fewer nuclei will be active (eg Huffman 1973). To model this dependence we define T as the temperature at which the prevailing humidity would correspond to water saturation. The deposition nucleation rate is given by

$$\frac{dn_{si}}{dt} = f G \gamma(\bar{T}) \cdot \frac{d\bar{T}}{dt} \qquad (13)$$

Droplets frozen homogeneously, or by condensation freezing, are assigned to adjacent ice crystal size bins (in general there will be no crystal bins of exactly the same size because of the different growth rates) in such a way that number concentration is conserved:

$$\frac{d}{dt} \sum_i (n_{si} + n_{Li}) = 0 \qquad (14)$$

Total condensed water mass is also conserved by distributing frozen droplets to crystal bins both smaller and larger in size in suitable ratios. Deposition nucleation does not affect the droplet distribution but merely nucleates new crystals. These are assigned to the smallest available crystal size bin. The number of ice crystal bins in the model is fixed.

Because crystal growth rates are much larger than droplet growth rates a situation soon arises where the radii associated with the crystal size bins are larger than all the droplets, making the above conservation impossible. This is overcome by retaining a number of 'inactive' bins of small radius and releasing them at suitable intervals. When the supply of inactive bins is exhausted the entire crystal spectrum is re-allocated to fewer bins, releasing more spare bins.

Once ice crystals have been nucleated they grow according to the usual growth rate formula

$$\frac{dm_{si}}{dt} = \frac{4\pi C \sigma_s}{\left\{ \frac{L_s}{kT}\left(\frac{L_s w_L}{RT} - 1\right) + \frac{RT}{D w_L e_s^{sat}(T)} \right\}} \qquad (15)$$

(Mason 1971, equation 5.4). Mass is used as a size variable to avoid the singularity in dr_{si}/dt at $r_{si}=0$. C is the crystal "capacitance", defined by the electrostatic analogy with the diffusion equation. In the model we simply assume spherical crystals for which C = r. Crystals of other geometries will also have a capacitance proportional to a characteristic dimension. We have not made a study of how crystal shape effects the conclusions below but preliminary results suggest that they are not highly sensitive to C. The effects of surface curvature on vapour pressure are ignored. Note that this approximation could not be made in equation (2) because the growth of cloud droplets is determined by the balance between the curvature term and the saturation ratio. This is not the case for ice crystals which are normally growing by diffusion at appreciable ice supersaturation.

Finally we must supply the initial conditions. This is done by specifying the parcel dew point, Td, and the updraught velocity, w. The starting temperature of the parcel is usually assumed to be the frost point.

The above equations form a closed set of coupled non-linear differential equations. If the model is run with NL CCN/droplet bins and Ns crystal bins we require 2(NL+NS) dependant variables for the sizes and concentrations, together with three thermodynamic variables (σ_s, σ_L, T) and three variables for the total number of nucleations of each type. The independent variable is time, t. This set of equations is solved numerically using a simple predictor-corrector method with fixed step-length, Δt. This is found to be sufficiently robust and efficient. By repeating runs with various step lengths we find that $\Delta t = 0.5s$ is sufficiently short to give accurate solutions. 64 bit precision arithmetic is used to avoid rounding errors.

It can be shown that the equilibrium radius of a haze droplet with respect to the ambient saturation ratio is maintained with a time constant given by

$$\tau_h = \frac{\Gamma_L \, r_{Li}^3}{\left(\frac{3 c m_N}{r_{Li}^2} - \frac{b}{T} \right)} \qquad (16)$$

When this is shorter than the numerical timestep instability sets in. To avoid this a damping factor is applied to the growth rate. This has no effect on the solution and is merely a device for keeping haze droplets in equilibrium without changing the form of the equations we are solving. As the condensation level is approached τ_h increases

and the damping is removed.

Freezing often occurs very rapidly because of the strong temperature dependence of nucleation rates and the rapid growth of the resulting ice crystals. Unfrozen droplets quickly evaporate as the humidity falls. This results in large negative values for dn_{Li}/dt and dr_{Li}/dt. If n_{Li} and r_{Li} decrease with a time constant less than Δt they achieve negative values in our scheme and numerical instability sets in. To avoid having to use a very short step we again adopt a damping factor, applied to dn_{Li}/dt and dr_{Li}/dt when necessary. By performing test runs of the model with a very short timestep, we have found that runs with the damping factor in operation, and a larger time step, do indeed converge to the correct solution. A further check on the accuracy of the solutions is the degree to which water and heat are conserved. Both of these are conserved to an accuracy of better than 0.1% when the time step is set to 0.5 s.

The model is usually run with five CCN/droplet sizes, initially spaced logarithmically between 0.03 um and 3.0 um radius. This range was chosen because nuclei smaller than .03 um are hardly ever activated, even in the absence of ice, whereas larger nuclei are too few to affect the results. Sample runs with 10 sizes spanning the same range lead us to believe that finite resolution of the spectrum does not materially affect the conclusions drawn below.

3. RESULTS

a) Ice Crystal Spectra

The model may of course be run with three nucleation modes simultaneously but first it is helpful to consider each separately. The number concentration results in this section are valid when the temperatures are below the thresholds discussed in sections 3.2 and 3.3.

i) Homogeneous nucleation

Results from a sample run are shown in Figure 1. The left-hand part of Figure 1 (a) shows the familiar pattern of haze growing into cloud droplets at the condensation level, 300m above the start of the run. The smallest CCN remain inactive while the rest of the spectrum grows and narrows. Soon after condensation the water supersaturation peaks at about 0.6% and thereafter falls gradually. The liquid water content (LWC) grows approximately adiabatically. As the droplets grow and cool the nucleation rate predicted by (9) increases rapidly and the number of crystals nucleated rises, as shown in Figure 1 (d). Eventually there are sufficient crystals to consume vapour faster than it is being released by ascent. The saturation ratio starts to fall, droplets evaporate and no further nucleation can occur.

Results for the final number of crystals nucleated under various conditions are shown in Figure 2 and are fitted by:

$$N_{xh} = 6.7 \times 10^{6} \; w^{1.6} \quad (m^{-3}) \qquad (17)$$

N_{xh} depends mainly on updraught and hardly at all on temperature or CCN concentration. This is surprising in view of the rapid variation of nucleation rate with temperature. It occurs because the main factor determining N_{xh} is the rapid growth of the first crystals to be nucleated. For a typical cirrus updraught of 0.5 ms^{-1} homogeneous nucleation yields 10^{6} crystals m^{-3} whereas 10^{8} cloud droplets condense. Only one in 10^{2} droplets freeze. We estimate that updraughts of the order of $10ms^{-1}$ are needed to freeze the entire droplet spectrum.

Most crystals are nucleated within a few 10's seconds which results in a sharply peaked spectrum (Figure 3). Because nucleation usually occurs close to water saturation, and always at appreciable ice super-saturation, these initial ice crystals continue to grow rapidly until they reach an equilibrium size when the ice saturation is close to zero. This occurs on a timescale of a few minutes. The final size is thus determined by the difference in saturation vapour densities over water and ice, together with the number of ice crystals. Further growth may only occur by sedimentation (which is not considered) or continued ascent. Typical equilibrium sizes and timescales are shown in Table 1. Note that the growth-rate equation (15) always works to narrow the spectrum which therefore remains sharply peaked.

ii) Condensation-freezing

The results obtained with this mode operative are very similar to homogeneous freezing. The final number of crystals nucleated is approximately

$$N_{xcf} = 4.5 \times 10^{6} \; w^{1.35} \quad (m^{-3}) \qquad (18)$$

Once again this is insensitive to nucleus concentration and temperature. Only a small fraction of the available $\nu(T)$ nuclei are used, before evaporation causes nucleation to cease, and so this term in (12) is unimportant. The ways in which nucleation rate depends on droplet volume and molarity of ammonium sulphate are similar to homogenous nucleation, which presumably explains the similarity of (17) and (18). To avoid depletion of the ice crystal concentration relative to the Fletcher distribution large updraughts are needed. At -40°C, for example, N_{xcf}, given by (18), equals $\nu(T)$ when $w=20ms^{-1}$.

ii) Deposition nucleation.

Deposition nucleation yields rather fewer crystals. Figure 4 shows some results for N_x which are fitted by:

$$N_{xd} = 6.6 \times 10^{5} \; w^{1.45} \quad (m^{-3}) \qquad (19)$$

The linear fit is so much better than Figure 2 because of the smooth way in which the deposition nucleation rate varies with saturation

ratio. Homogeneous nucleation rates increase very rapidly as droplets condense (see section 4). Figure 4 also shows how insensitive the results are to nucleus concentration. A depletion of f = 10^{-2} yields only a 30% change in N_{xd}.

The mean radii of initial crystals are given in Table 2 which shows slightly larger sizes than Table 1. This is the result of two competing effects: lower values of N_{xd} ,tending to produce larger crystals; and nucleation occurring at lower humidities, tending to produce smaller crystals. Lower number concentration also prolongs the timescale, τ, of the freezing process.

b) Dominant Nucleation Modes

The maximum saturation ratio achieved in air of dew point T_d is given by

$$\sigma_{Lm} = A\,(T_d - T_l) \quad (T_d > T_l) \tag{20}$$

where

$$T_l = \alpha w^{\beta} \tag{21}$$

These formulae were obtained from peak saturation ratios observed in a large number of model runs. Some results illustrating this fit are shown in Figure 5. The temperature T_l represents a critical dew point below which cloud droplets fail to condense before freezing sets in. The constants A, α, β depend on nucleation mode and are shown in Table 3.

Although (20) is a fit to numerical results T_1 may also be calculated for heterogeneous nucleation modes by equating N_x (given by (18) or (19)) with $\nu(T)$ given by the Fletcher distribution (1). The effects of depleting $\nu(T)$ by a factor f may thus be assessed without repeating a large number of model runs. Lower nucleus concentrations move the corresponding curve in Figure 5 to the left.

The model results for peak values of the water saturation ratio shown in Figure 5 may be used to determine which mode of nucleation dominates in a given circumstance. If the peak saturation ratio corresponding to mode X (say) is not reached because nucleation by another mode, Y, has occurred at a lower humidity, then mode Y will always dominate. Crystals nucleated by mode Y will prevent the humidity rising sufficiently to nucleate a significant number of crystals by mode X. The numbers and sizes of ice crystals nucleated will be characteristic of Y. This situation occurs when the curve in Figure 5 corresponding to Y lies below that corresponding to X. Note that situations where two or more nucleation modes are contributing are rare. The modes interact so strongly that one mode completely swamps the others.

Figure 5 shows that deposition nucleation (un-depleted, f=1.0) is normally the dominant mode and that homogeneous freezing and condensation freezing remain inactive. However when deposition nuclei are depleted the corresponding peak saturation curve moves to the left. For example when the depletion ratio, f, is 10^{-3} the deposition curve crosses the homogeneous curve at -42°C. Above this temperature homogeneous freezing occurs whereas below it deposition nucleation

sets in. Because more crystals are nucleated homogeneously (equations (17), (18)), this change-over at -42°C gives rise to the unexpected result that fewer crystals may be nucleated at lower temperatures. This is illustrated by the numerical results shown in figure 6. Change-over temperatures for other updraughts and depletion factors are shown in Figure 7.

Figure 5 also shows that condensation-freezing dominates homogeneous freezing throughout the temperature range considered. However due to the similar numbers of crystals nucleated in the two modes, and the similar saturation ratios achieved, it is immaterial which is actually occurring (except perhaps in the discussion of liquid water in Section 3.3) and cloud physics measurements are unlikely to distinguish them. Because of the similarity of the peak saturation curves for condensation-freezing and homogeneous freezing, Figure 7 is also a good guide to the change-over temperature between deposition nucleation and condensation freezing.

b) Liquid Water

i) Homogeneous freezing.

Model runs show a homogeneous freezing threshold temperature T_h:

$$T_h = -35.0\ w^{0.025} \qquad (22)$$

Roughly speaking, parcels with a dew point warmer than this will form normal water cloud at the condensation level. This will freeze

suddenly when T_h is reached. The precise value of the freezing temperature depends somewhat on parcel history (for example a parcel with a high dew point will tend to freeze at a lower temperature due to the larger quantity of liquid water to be frozen) but (22) is generally accurate to approximately +- 1°C. Note that T_h is several degrees warmer than the frequently quoted homogeneous freezing threshold of -40°C because only a small fraction of the droplet population actually freezes. Parcels with a dew point lying between the liquid water threshold, T_l , and the homogeneous freezing threshold, T_h, display a transient liquid water phase typically lasting for about 1 minute. This region is shown on Figure 7. Below T_l haze droplets freeze homogeneously.

We may calculate the lifetime with respect to homogeneous freezing of a population of cloud droplets. Assuming a liquid water content of $0.5 \times 10^{-4} kgm^{-3}$ (approximately 100m ascent adiabatic LWC at -25°C) and that freezing is complete when 10^6 crystals have formed, (9) gives the lifetimes shown in Table 4. We conclude that water cloud warmer than -33°C will not freeze homogeneously. For temperatures below -35°C the transient water phase between T_l and T_h is longer lived than the timescales in the table and is therefore maintained by fresh condensation.

ii) Condensation-freezing.

Condensation freezing is limited both by droplet volume and by the total number $\nu(T)$ nuclei available. When liquid water condenses droplet volume ceases to be a restriction and all the $\nu(T)$ nuclei

are activated. Further crystals may only form as the temperature falls. Droplets evaporate when the crystals consume vapour faster than ascent releases it. It turns out that this condition depends mainly on how many crystals are present and thus occurs at some well-defined temperature, T_I . Thus above T_I water cloud is meta-stable with respect to condensation-freezing whereas at lower temperatures liquid water does not occur and haze droplets freeze.

The time taken by $\nu(T)$ crystals to evaporate LWC kgm^{-3} of liquid water is:

$$\tau_f = \frac{1}{2\sigma_s \Gamma_s} \left(\frac{3\ LWC}{4\pi \rho_L \nu(T)} \right) \qquad (23)$$

where Γ_s is the denominator in the growth-rate equation (16). Using $LWC = 0.5 \times 10^{-4} kgm^{-3}$, $\Gamma_s = 2.0 \times 10^{-11} m^2 s^{-1}$, and $\sigma_s = 0.25$ we obtain the lifetimes in Table 5. This shows that water cloud warmer than T_I may have a lifetime of only a few minutes. Also, because the lifetimes vary more slowly than for homogeneous nucleation there is a larger range of temperatures (say from -22°C to -32°C) over which such meta-stable cloud occurs.

iii) Deposition nucleation.

Because T = T at water saturation, deposition nucleation also yields $\nu(T)$ crystals when liquid cloud forms, and the threshold temperature is similar to that for condensation-freezing. In fact T_I turns out to be slightly higher in this case because nucleation will have started long before cloud condensation occurs resulting in

larger (and therefore faster growing) crystals than condensation-freezing. At temperatures above T_1 meta-stable water cloud occurs, as described above. Below T_1 deposition nucleation prevents water cloud condensing.

4. ANALYTIC APPROXIMATION

It is interesting to examine which features of the nucleation parametrization produce results exemplified by equations (17) to (21), particularly in view of our uncertainty of these parametrizations. It is possible to understand some of the features of the above results by considering a simplified version of the problem of deposition nucleation and obtaining an approximate analytic solution. Suppose that the number of active nuclei at time t depends on the ice supersaturation as follows:

$$N(t) = B\sigma_s(t)^{\theta} \qquad (24)$$

Huffman (1973) found experimental values for θ between 3 and 8. This description of the deposition nucleus distribution differs from equation (13), but the two are related by the Clausius-Clapeyron equation and are approximately equivalent over narrow temperature ranges. Comparing (24) and (13) in the temperature range -30°C to -35°C gives θ =17. The range -45°C to -50°C gives θ =24. The corresponding values for B are $6.8\times10^{13}\,m^{-3}$ and $1.6\times10^{16}\,m^{-3}$.

The saturation ratio given by equation (6) may be written in the simplified form:

$$\sigma_s(t) = \chi w t - \lambda \bar{r}^3(t) N(t) \qquad (25)$$

where χ and λ are slowly varying functions of temperature and are regarded as constants in the calculations below. Comparison with (6) gives $\lambda = 10^7$ at -30°C and 10^8 at -50°C; and $\chi = 10^{-3} m^{-1}$. Similarly we may simplify the crystal growth equation (15) to:

$$\frac{dr}{dt} = \frac{\sigma_s \Gamma_s}{r} \qquad (26)$$

where the 'constant' Γ_s is $8 \times 10^{-12} m^2 s^{-1}$ at -30°C and $2 \times 10^{-12} m^2 s^{-1}$ at -50°C. This integrates to

$$r(t',t) = 2\Gamma_s \int_{t'}^{t} \sigma_s(\tau)\, d\tau \qquad (27)$$

where r(t',t) is the radius at time t of a crystal nucleated at time t'. Moments of the size spectrum are then given by:

$$\bar{r}^n(t) = \frac{1}{N(t)} \int_0^t \frac{dN(t')}{dt'} \left\{ 2\Gamma_s \int_{t'}^{t} \sigma(\tau)\, d\tau \right\}^{n/2} dt' \qquad (28)$$

It is assumed that $dN(t)/dt >= 0$. The set of coupled equations (24),(25), and (28) may be solved by iteration. For an initial guess at the solution take

$$\sigma_s(t) = \chi w t \qquad (29)$$

Feeding this into (28) and making the approximation $\overline{r^2} = \left(\overline{r^3}\right)^{2/3}$ to simplify the algebra we obtain

$$\overline{r^3} \simeq \gamma t^3 \tag{30}$$

where

$$\gamma = \left(\frac{2\Gamma_s \chi_w}{\theta+2}\right)^{3/2} \tag{31}$$

Now when N and σ_s reach their peak values, at $t=t_m$ say, we have

$$\left.\frac{dN(t)}{dt}\right|_{t=t_m} = \left.\frac{d\sigma_s(t)}{dt}\right|_{t=t_m} = 0 \tag{32}$$

and so differentiating (25):

$$\chi_w - 3\lambda\gamma t_m^2 N(t_m) = 0 \tag{33}$$

which gives

$$N(t_m) = B^{\frac{1}{1+\theta/2}} \left(\frac{2}{3}\right)^{\frac{\theta}{1+\theta/2}} (\chi_w)^{\frac{3\theta}{4+2\theta}} \left(\left(\frac{\theta+2}{2\Gamma_s}\right)^{3/2} \frac{1}{3\lambda}\right)^{\frac{\theta}{2+\theta}} \tag{34}$$

θ is sufficiently large for us to simplify this to:

$$N(t_m) = \frac{\sqrt{2}}{27} \frac{1}{\lambda} B^{2/\theta} (\chi_w)^{3/2} \left(\frac{\theta+2}{\Gamma_s}\right)^{3/2} \tag{35}$$

If we wished we could use (30) and (25) to give an improved guess for

σ_s and repeat the iteration.

This expression for N reproduces the dependence of N_x on $w^{3/2}$. Also, N is insensitive to changes in the nucleus distribution. For example, if θ=10. then an order of magnitude change in B gives a 60% change in N_x. Changing θ has a greater effect, but because this is an exponent of the distribution we would expect it to be less variable. Using the values θ = 17 and θ = 24, together with the values for χ, λ, and B stated above we find that in the range -30°C to -35°C

$$N_x = 4.5 \times 10^6 \; w^{3/2} \tag{36}$$

and in the range -45°C to -50°C

$$N_x = 7.0 \times 10^6 \; w^{3/2} \tag{37}$$

This weak temperature dependence partly results from changes in λ and Γ_s working in opposite senses.

We believe the above theory also applies to condensation-freezing and homogeneous nucleation. In these cases the nucleation rate is a very rapidly varying function of saturation ratio for a narrow range of humidity near the condensation level and is determined by the volume of the haze/cloud drops rather than the number of active nuclei. The effective θ is presumably much larger than for deposition nucleation resulting in more crystals being nucleated. However the other features of the solution are similar.

We conclude that the features needed to produce results with the general characteristics seen in the previous section are firstly that updraughts are not so rapid that all the nuclei available at a given temperature are activated (when (23) would break down), and secondly that the nucleation rate increases rapidly with saturation ratio.

5. SUMMARY AND DISCUSSION

The most important results of this paper are summarised by (17) to (19), namely:

i) Only a small fraction of available nuclei produce ice crystals in cirrus updraughts. A vertical velocity of $10ms^{-1}$ or more is required to freeze all the droplets or activate all the deposition nuclei. Thus we do not need to postulate a shortage of ice nuclei at cirrus levels to explain the low crystal concentrations.

ii) The number of crystals nucleated depends on approximately the 3/2 power of the updraught velocity.

iii) The number of crystals nucleated in the model does not depend strongly on temperature (in contrast to what we might expect from the Fletcher distribution (1) or the homogeneous freezing rate (9)) which explains why observed cirrus crystal concentrations do not appear to increase with altitude (Rangno and Hobbs 1986).

iv) The number of crystals nucleated by a given mode does not depend on the details of the corresponding nucleus distribution.

The threshold dewpoints discussed in section 3.2 do however depend on nucleus distributions and are of interest because they tell us when liquid water may be present. We predict that when no

heterogeneous nuclei are present water cloud is stable above -33°C and this represents an upper limit for cirrus cloud top temperature. Transient liquid water may be present down to -39°C and below this temperature haze droplets freeze homogeneously. This transient phase is rather short-lived. On the other hand if ice nuclei are present in concentrations given by (1) homogeneous freezing is suppressed. Above -22°C water cloud has a lifetime of more that 1 hour, but between -22°C and -32°C the liquid water is a transient phase, although longer-lived than the transient phase in homogeneous freezing. Nucleus depletion lowers these thresholds. These results show the need for more observations of when liquid water occurs, in order to distinguish nucleation modes. At present observations suggest that it exists at -36°C whence Figure 7 predicts that deposition nuclei are depleted by a factor of 3×10^{-3} or less.

Peak saturation ratios, given by (19), should also help distinguish nucleation modes. Very little data for humidity in cirrus is available because of the slow response of instruments like the Cambridge hygrometer. We hope that Lyman-α probes will remedy this by producing fast response measurements of peak humidity.

The sizes of initial ice crystals predicted by Table 1 are on the limit of detection by PMS 2d probes, which may therefore undercount. We agree with Rangno and Hobbs that instrument response may be an additional factor in low cirrus concentration measurements. Indeed, whilst (17) and (18) predict far fewer crystals than nuclei they nevertheless yield somewhat higher concentrations than are typically observed. There is clearly a need for improved understanding of the response of existing optical probes to small ice

crystals. Because the model only yields sharply peaked crystal spectra our results are only applicable to peak concentrations of small crystals. The broad, approximately exponential, size spectra frequently observed in cirrus occur by mechanisms we have not considered.

Heymsfield and Platt (1983) present parametrizations for number concentrations and condensed water content in cirrus based on a large number of observations. These suggest that concentrations decrease by an order of magnitude or so as the temperature falls below -40°C. This is in excellent agreement with Figure 6. Heymsfield and Platt also note a corresponding change in crystal habit from spatials to pristine crystals, which would be consistent with a change of nucleation mode.

Another explanation for lower concentrations at lower temperatures is the dependence on updraught velocity. We expect this to be lower at colder temperatures because less latent heat is available to generate buoyancy. This is also borne out by Heymsfield and Platt. The dependence of concentration on updraught also provides strong coupling between the microphysics and dynamics which we have largely ignored by assuming a constant updraught. There is clearly scope for treating updraught as a dependent variable calculated from buoyancy (cf Mason and Emig 1961).

We hope that in its present form the model will provide a much-needed framework for interpreting aircraft observations of ice crystal spectra, liquid water, humidity and updraught velocity. For example it will be instructive to search for a correlation between peak updraught velocity and peak crystal concentration. Improved data

on nucleus distributions and properties should be easy to incorporate into the model. These studies will enable us to commence work on the development of cloud-scale cirrus models with a sound microphysical basis.

REFERENCES

Baumgardner D., Dye J.E., and Cooper W.A. 1986

The effects of measurement uncertainties on the analysis of cloud particle data.

Jt. sess. 23rd Conf Radar Met. Conf Cloud Phys 3 JP313-JP316

Beard K.V. and Pruppacher H.R. 1971

A wind tunnel investigation of the rate of evaporation of small water drops falling with terminal velocity in air.

J. Atmos. Sci. 28 1455-1464

Bigg E.K. 1963

Cross sections of ice nucleus concentrations at altitude over long paths.

J. Atmos. Sci. 24 226

Bigg K. and Meade R.T. 1971

High level stratocumulus clouds.

Weather 26 55-57

Bigg E.K. and Miles R.T. 1963

Stratospheric ice nucleus measurements from balloons.

Tellus 162-166

Brown P.R.A. and Darlison A.G. 1988

The comparison of holographic and 2-D probe measurements of ice

crystals.

Proc. 10th Int. Cloud Phys. Conf.

Eadie W.J. 1971

A molecular theory of the homogeneous nucleation of ice from supercooled water.

Tech note £ 40 Cloud Physics Laboratory, Univ. Chicago.

Fletcher N.H. 1962

The physics of rainclouds.

Cambridge University Press.

Gorbunov B.Z., Kakutkina N.A., Koutzenogii K.P., Pashenko A.E., and Safatov A.S. 1987

Kinetics of ice nucleation on aerosol particles in supercooled fog.

J. Aerosol Sci. 18 £3 261

Hall D. and Pruppacher H.R. 1976

The survival of ice particles falling from cirrus cloud in subsaturated air.

J. Atmos. Sci. 33 1995-2006

Heymsfield ,A.J. 1975

Cirrus uncinus generating cells and the evolution of cirriform cloud. Part I. Aircraft observations of the growth of the ice phase.

J. Atmos. Sci.32 799-808

Heymsfield A.J. 1977

Precipitation development in stratiform ice clouds: a microphysical study.

Conf. Cloud Phys. 2 20-23 Boston, AMS

Heymsfield A.J. and Knollenberg R.G. 1972

Properties of cirrus generating cells.

J. Atmos. Sci. 29 1358-1366

Heymsfield A.J. and Platt C.M.R. 1983

A parameterisation of the particle size spectrum of ice clouds in terms of the ambient temperature and water content.

J. Atmos. Sci. 41 5 846

Howell W.E. 1949

Growth of cloud drops in uniformly cooled air.

J. Met. 6 134

Huffman P.J. 1973

Supersaturation spectra of AgI and natural ice nuclei.

J. App. Met. 12 1080-1082

Junge C. and McLaren E. 1971

Relationship of cloud nuclei spectra to aerosol size distributions and composition.

J. Atmos. Sci. 28 382-390

Knollenberg R.G. 1972

Measurements of the growth of,the ice budget in a precipitating contrail.

J. Atmos. Sci. 29 1367-1374

Kuhns I.E. and Mason B.J. 1968

The supercooling and freezing of small water droplets in air.

Proc. Roy. Soc. A302 437-452

Mason B.J. 1971

The physics of clouds.

Oxford University Press.

Mason B.J. and Emig R. 1961

Calculations of the ascent of a saturated bow parcel with mixing.

Quart. J. R. Met. Soc. 87 212(133)

Pruppacher H.R. and Klett J.D. 1978

Microphysics of cloud and precipitation.

D. Reidel.

Rangno A. and Hobbs P.V. 1986

Deficits in ice particle concentrations in stratiform clouds with top temperatures < -30°C

Rosinski J., Haagensen P.L., Nagamoto C.T., and Parungo F. 1986

Nature of ice forming nuclei in maritime airmasses.

J. Aerosol. Sci. 18 3 291-309

Sassen K. 1984

Deep orographic cloud structure and composition derived from comprehensive remote sensing measurements.

J. Climate Appl. Meteor. 23 569-583

Smithsonian Meteorological Tables, List,R.J (ed) 1984

Smithsonian Inst. Press.

Varley D.J. 1978

Air force surveys in geophysics #394. Cirrus particle distribution study part 1.

AFGL TR 78 0248.

Air Force Geophysical Laboratory.

APPENDIX 1. DEFINITIONS OF χ AND λ IN EQUATION (26)

Equation (6) may be simplified by making the following assumptions:

i) No liquid water is present ($d\omega_l/dt = 0.$)

ii) e_s^{sat} is approximated by the Clausius-Clapeyron equation

$$\frac{de_s^{sat}}{dT} = \frac{\epsilon L_s e_s^{sat}}{R_a T^2} \tag{A1}$$

iii) The term $(1+\sigma_s)$ on the right hand side of (6) may be treated as unity.

iv) Latent heat may be neglected:

$$\frac{dT}{dt} \simeq -\frac{gw}{c_p} \tag{A2}$$

v) The hydrostatic approximation may be used:

$$\frac{1}{p}\frac{dp}{dz} \simeq \frac{g}{R_a T} \tag{A3}$$

Equation (6) then becomes

$$\frac{d\sigma_s}{dt} = \chi w - \lambda \frac{d}{dt} \sum n_{si} r_{si}^3 \tag{A4}$$

where

$$\chi = \frac{g}{R_a}\left\{\frac{\epsilon L_s}{c_p T} - \frac{1}{T}\right\} \tag{A5}$$

and

$$\lambda = \frac{P}{\epsilon e_s^{sat}} \left(\frac{4\pi}{3} \frac{\rho_s}{\rho_a} \right) \qquad \text{(A6)}$$

These are both relatively slowly varying functions of temperature. Regarding them as constant over the range under consideration allows us to integrate (A4) to give (26).

APPENDIX 2. GLOSSARY OF NOTATION

This list includes numerical values used in the model, where appropriate.

Note the following subscripts:

L	liquid water
S	ice
P	either ice or water
N	nucleus material (ammonium sulphate)

A	constant in equations (20)
B	parameter in theoretical IN distribution.
C	crystal 'capacitance'
D	diffusivity of water vapour in air
F	empirical constant in Fletcher distribution = 10^{-2} m^{-3}
G	empirical constant in Fletcher distribution = $-0.6^{o}C^{-1}$
I	homogeneous nucleation rate
J	Van t'Hoft factor (=2.0 for $(NH_4)_2SO_4$)
K_a	thermal conductivity of dry air

L_v, L_s	latent heats of vaporization and sublimation =2.603×10^6 Jkg^{-1}, 2.833×10^6 Jkg^{-1}
LWC	liquid water content
M	mole fraction of solute in droplet
N	number of ice crystals
N_x	final number of ice crystals (subscripts h, cf, d refer to different nucleation modes
R	universal gas constant = 8.314 J mol^{-1} K^{-1}
R_a	gas constant for dry air =287.04 $Jkg^{-1}K^{-1}$
S	solute freezing suppression term
T	temperature (absolute)
T_c	temperature (°C)
T_d	parcel dew point
T_l	liquid water threshold temperature
T_h	homogeneous freezing threshold temperature
$\bar{T}$	effective temperature for deposition nucleation
W_L, W_N	molecular mass of water and ammonium sulphate
b, c	constants in droplet growth rate equation (2) =3.464×10^7 Km, 6.5109×10^{-5} $kg^{-1}m^3$ for $(NH_4)_2SO_4$
C_p	specific heat of air at constant pressure = 1005. J $K^{-1}kg^{-1}$
e^{sat}	saturation vapour pressure
f	depletion factor of heterogeneous nuclei
g	acceleration due to gravity = 9.807 ms^{-1}
h	Planck's constant = 6.6252×10^{-34} Js
i	size bin index
k	Boltzmann constant = 1.3804×10^{-23} JK^{-1}
m	mass of droplet, crystal or nucleus

n	number concentration
p, p_0	atmospheric pressure, ambient, and sea-level
r	radius of droplet, crystal, or nucleus
t	time
v	volume of droplet, crystal, or nucleus
w	vertical velocity of parcel
w	mixing ratio
z	altitude
Γ	denominator in growth-rate equation
Δg	molecular exchange energy = 2.0×10^{-20} J
ΔG^*	critical embryo free energy
Δt	numerical timestep
$\sum N$	number of condensation-freezing events to date
α, β	constants in equations (21) and (22)
γ	variable in equation (31)
ϵ	ratio of molecular masses of water and air = 0.622
θ	parameter in theoretical IN distribution
λ	'constant' defined by equation (A6)
ν_L, ν_s	molecular number densities for water and ice = 3.343×10^{28} m^{-3} and 3.065343×10^{28} m^{-3}
ν	number of ice nuclei given by the Fletcher distribution
ς	shape factor for ice embryos
ρ_a	atmospheric density
ρ_L, ρ_s	density of water, ice = 1.0×10^3 kg m^{-3}, 0.9168×10^3 kg m^{-3}
$\sigma, \sigma_c, \sigma_M$	saturation ratio, critical sat. ratio, max. sat. ratio
τ	growth time of initial crystals

τ_{cf} time constant in condensation-freezing parametrization

τ_f glaciation time of water cloud

τ_h response time of haze droplet to changes in..

ϕ_{sl} ice/water interfacial free energy = 2.40×10^2 Nm^{-1}

χ 'constant' defined by equation (A5)

Figures

1. Various model parameters for air at a dew-point of -30°C ascending at 0.1 ms^{-1} as a function of height above the starting altitude of the parcel. It is assumed that only homogeneous nucleation occurs.

2. The number of ice crystals nucleated homogeneously as a function of updraught velocity for parcels with various dew-points and assuming a maritime CCN distribution of the form give n by Junge (1971). Also shown are data-points for a model run with CCN depleted by a factor of 10.

3. The differential ice crystal size spectrum at the completion of homogeneous nucleation for a parcel with a starting dew-point of -40°C and an updraught of 1.0 ms^{-1}.

4. The number of ice crystals nucleated by the deposition mode alone as a function of updraught velocity for parcels with a dew-point of -40°C, assuming the Fletcher (1962) IN distribution. Also shown are points corresponding to a depletion of the IN concentration by a factor of $f=10^{-2}$.

5. Numerical model results showing the peak value of the water saturation ratio, σ_{Lm} as a function of parcel dew-point for different nucleation modes. An updraught of 0.5 ms^{-1} has been assumed.

6. The number of crystals nucleated as a function of dew-point for model runs with both deposition and homogeneous nucleation active. Deposition nuclei are depleted by a factor of 10^{-3}.

7. The solid hatched curves indicate the threshold between homogeneous and deposiotion nucleation for various values of the deposition nucleus depletion factor, f. Parcels lying to the left of these curves freeze homogeneously whereas to the right they freeze by deposition nucleation. Also shown are the homogeneous nucleation threshold (dashed) and the homogeneous liquid water threshold (dotted). Transient liquid water occurs for parcels lying between these two curves.

Fig. 1

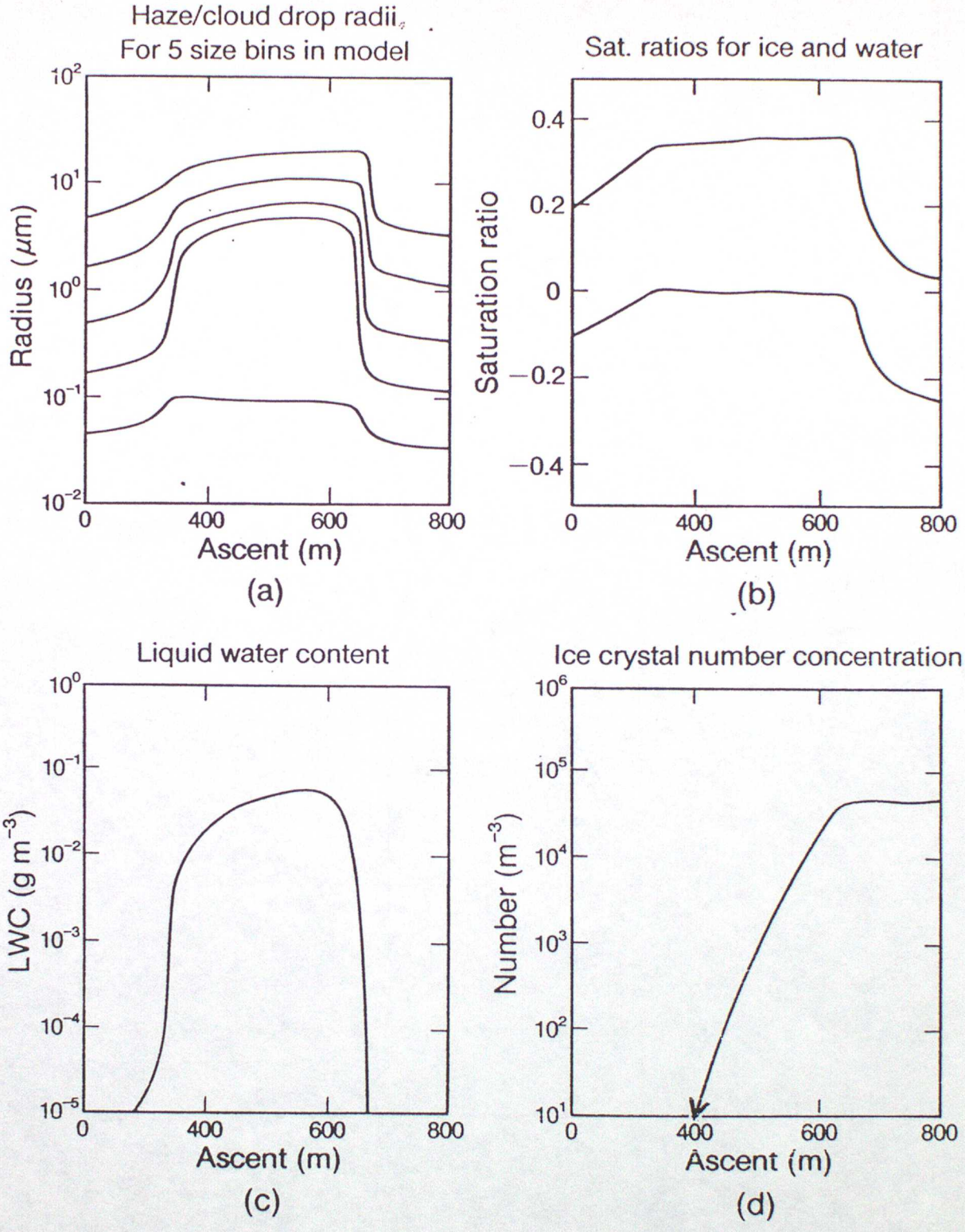
Haze/cloud drop radii
For 5 size bins in model
Radius (μm)
Ascent (m)
(a)
Sat. ratios for ice and water
Saturation ratio
Ascent (m)
(b)
Liquid water content
LWC (g m⁻³)
Ascent (m)
(c)
Ice crystal number concentration
Number (m⁻³)
Ascent (m)
(d)

Fig. 2.

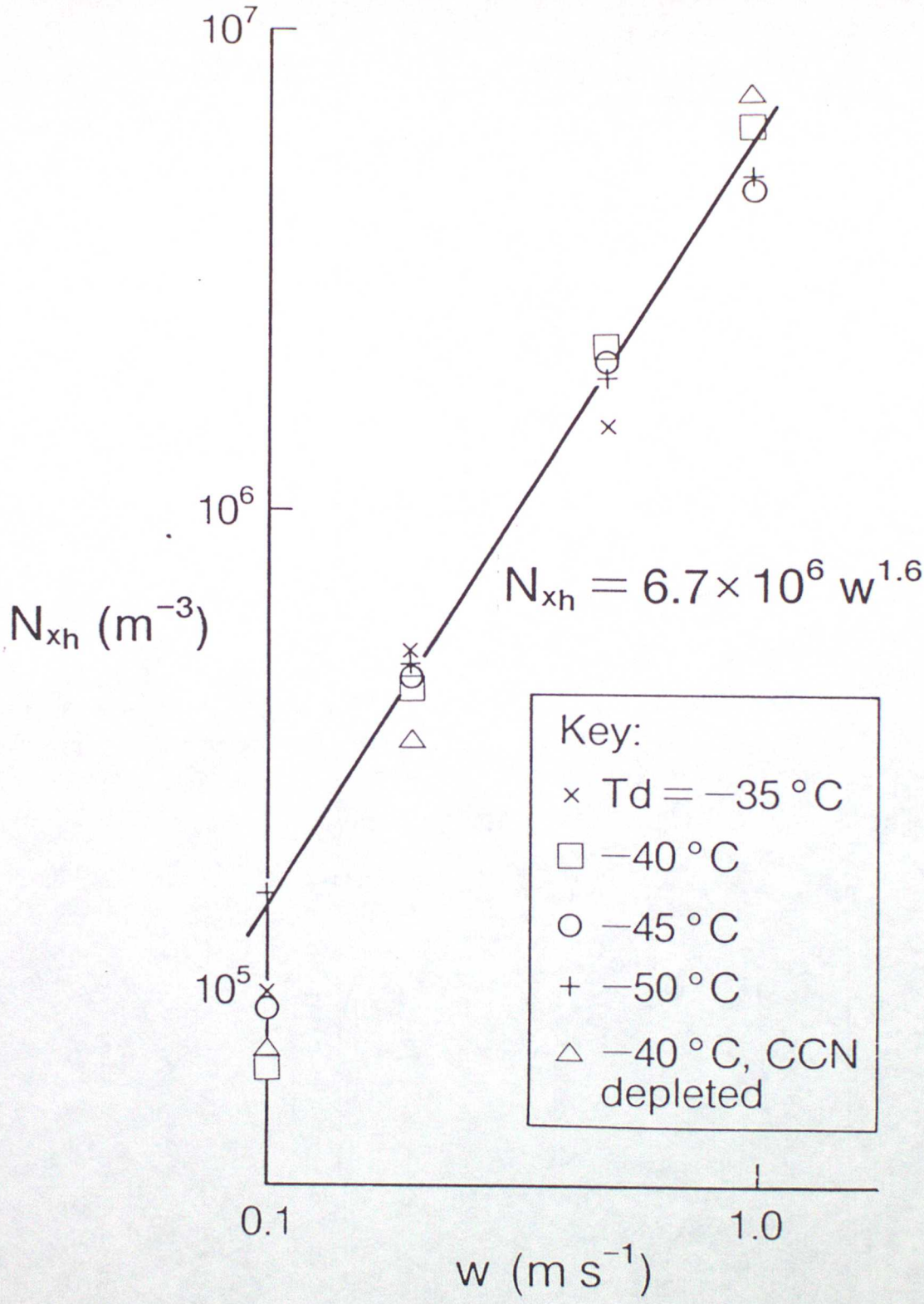
10^7
10^6
10^5
N_{xh} (m^{-3})
$N_{xh} = 6.7 \times 10^6\ w^{1.6}$
Key:
× Td = −35 °C
□ −40 °C
○ −45 °C
+ −50 °C
△ −40 °C, CCN depleted
0.1
1.0
w ($m\ s^{-1}$)

Fig. 3

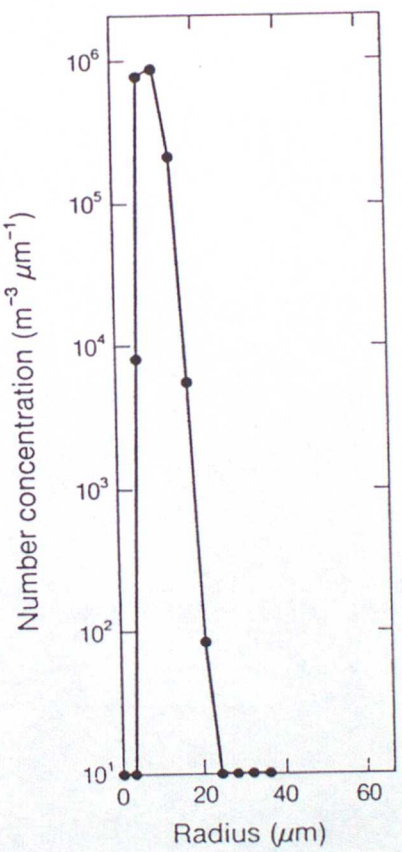
Number concentration (m^{-3} μm^{-1})
10^6
10^5
10^4
10^3
10^2
10^1
0
20
40
60
Radius (μm)

Fig. 4

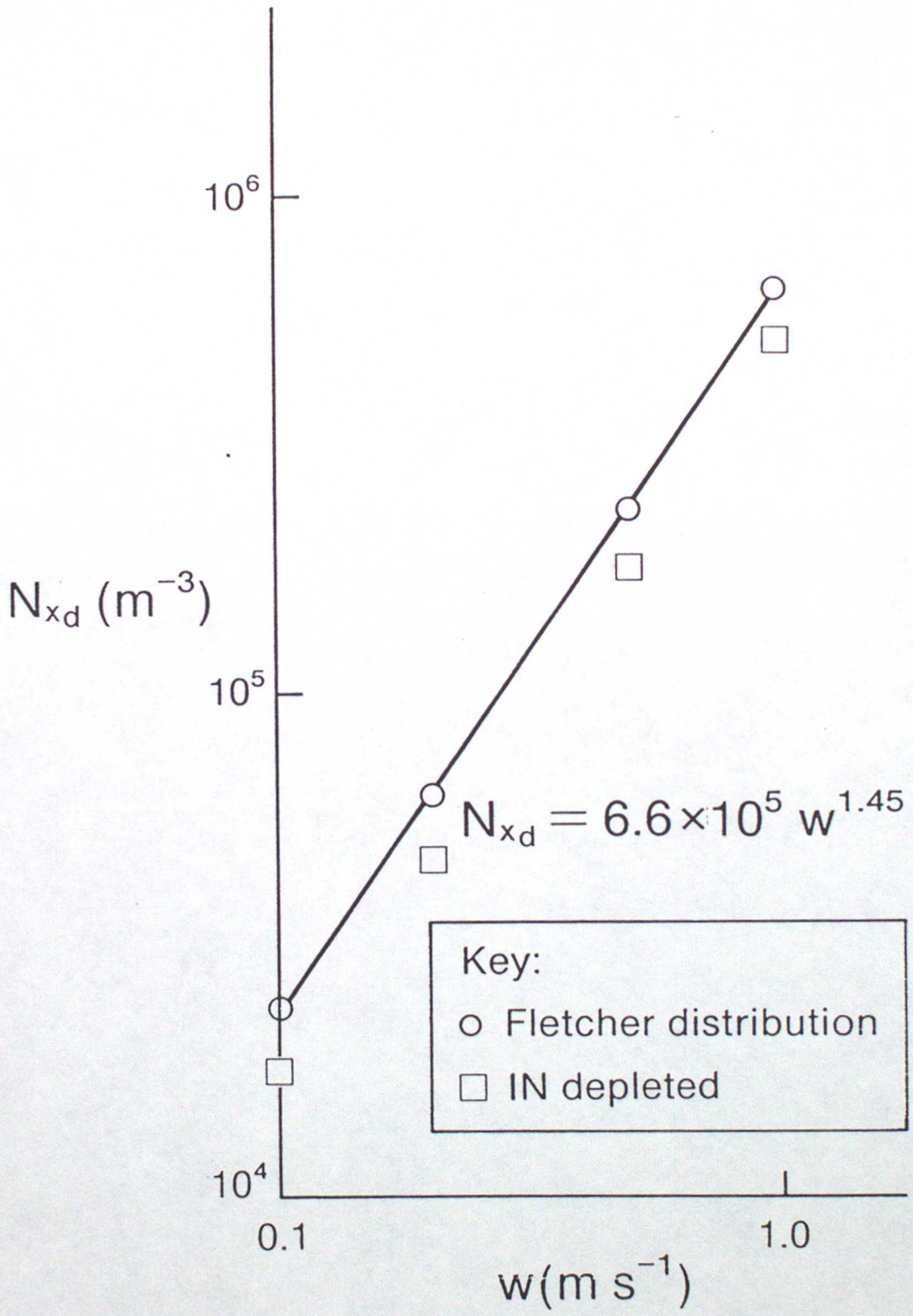
10^6
10^5
10^4
N_{xd} (m^{-3})
$N_{xd} = 6.6 \times 10^5\ w^{1.45}$
Key:
o Fletcher distribution
□ IN depleted
0.1
1.0
w($m\ s^{-1}$)

Fig. 5

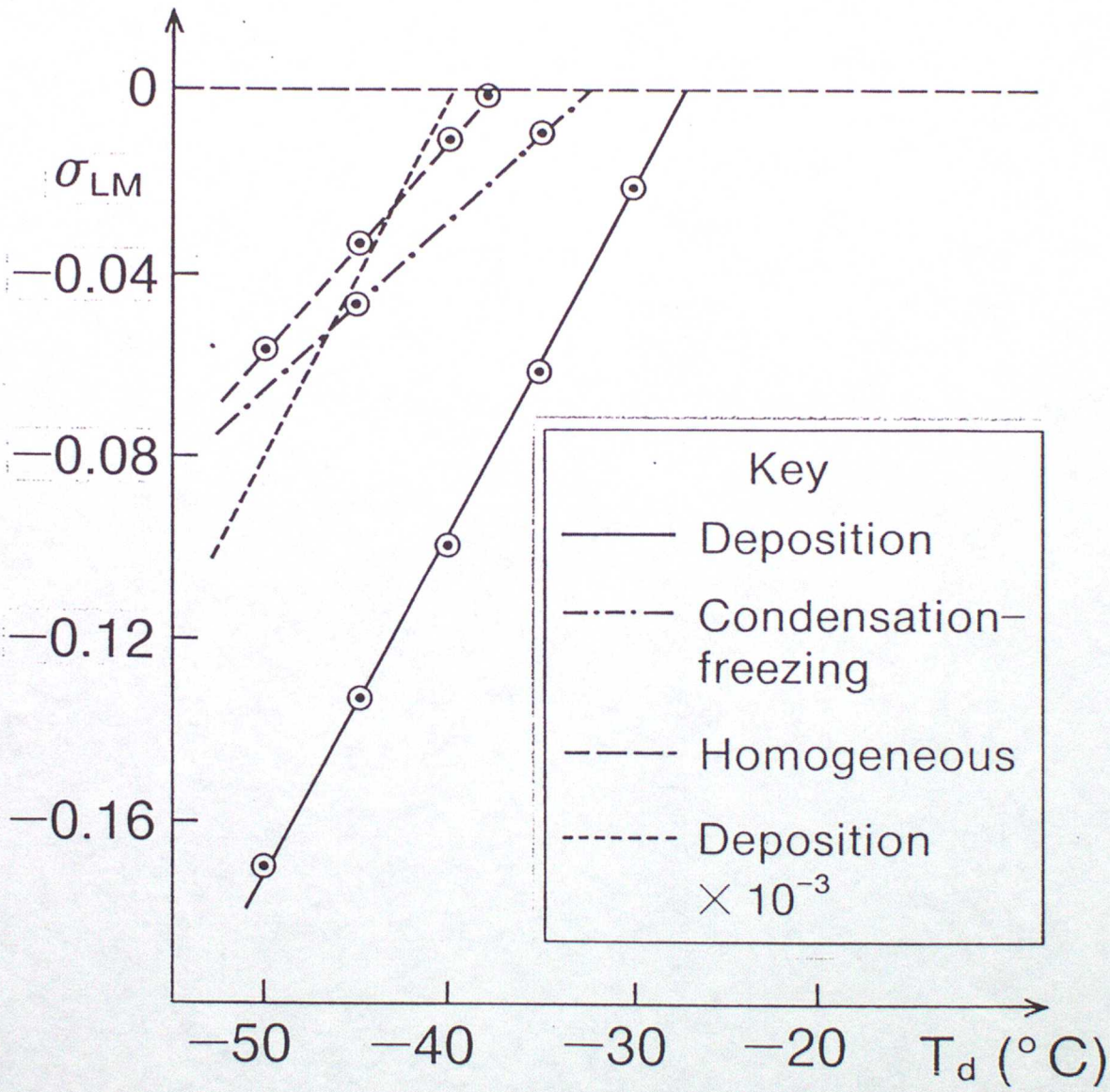
0
σ_{LM}
−0.04
−0.08
−0.12
−0.16
−50
−40
−30
−20
T_d (°C)
Key
Deposition
Condensation–freezing
Homogeneous
Deposition × 10^{-3}

Fig. 6

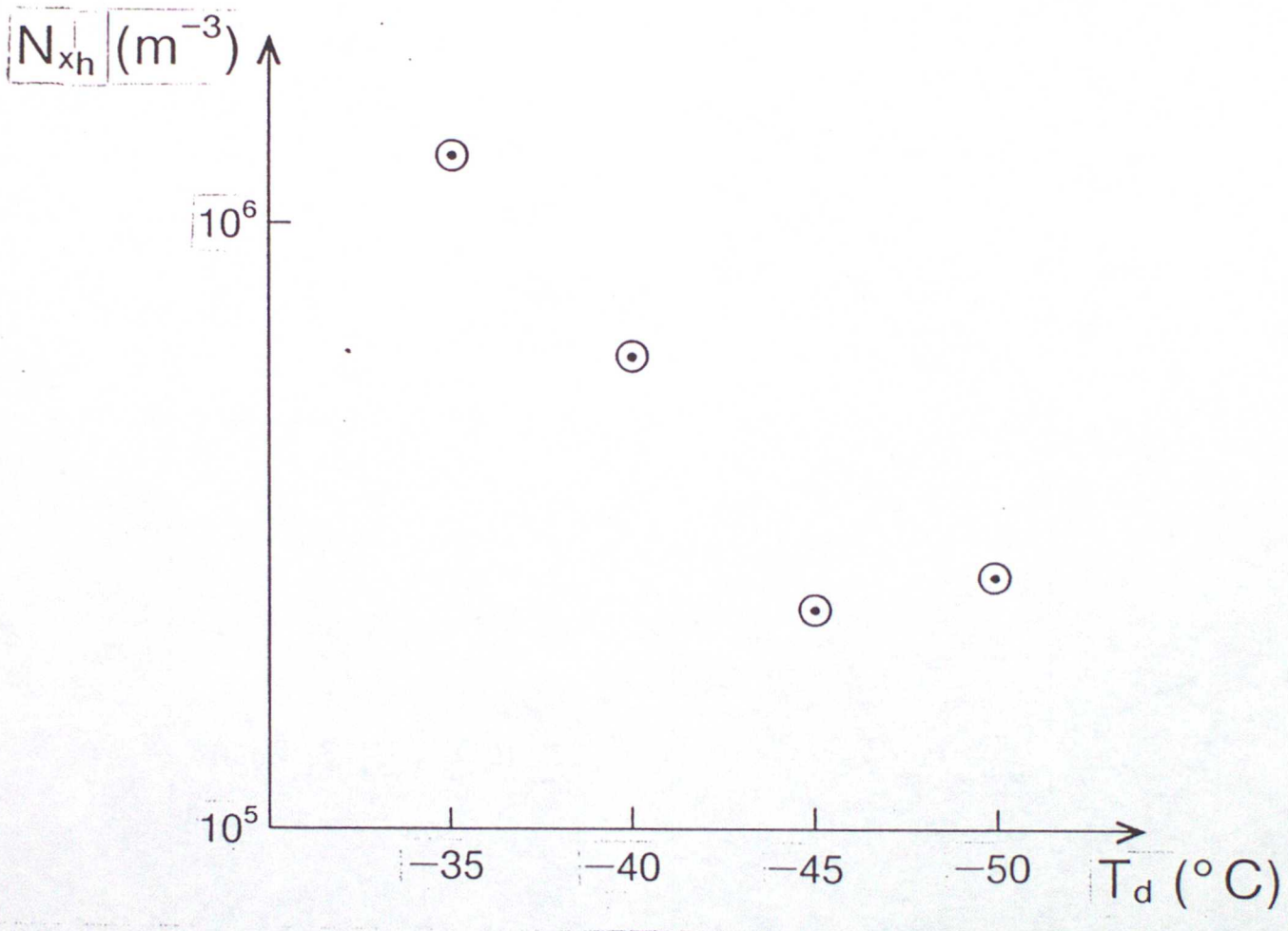

Fig. 7

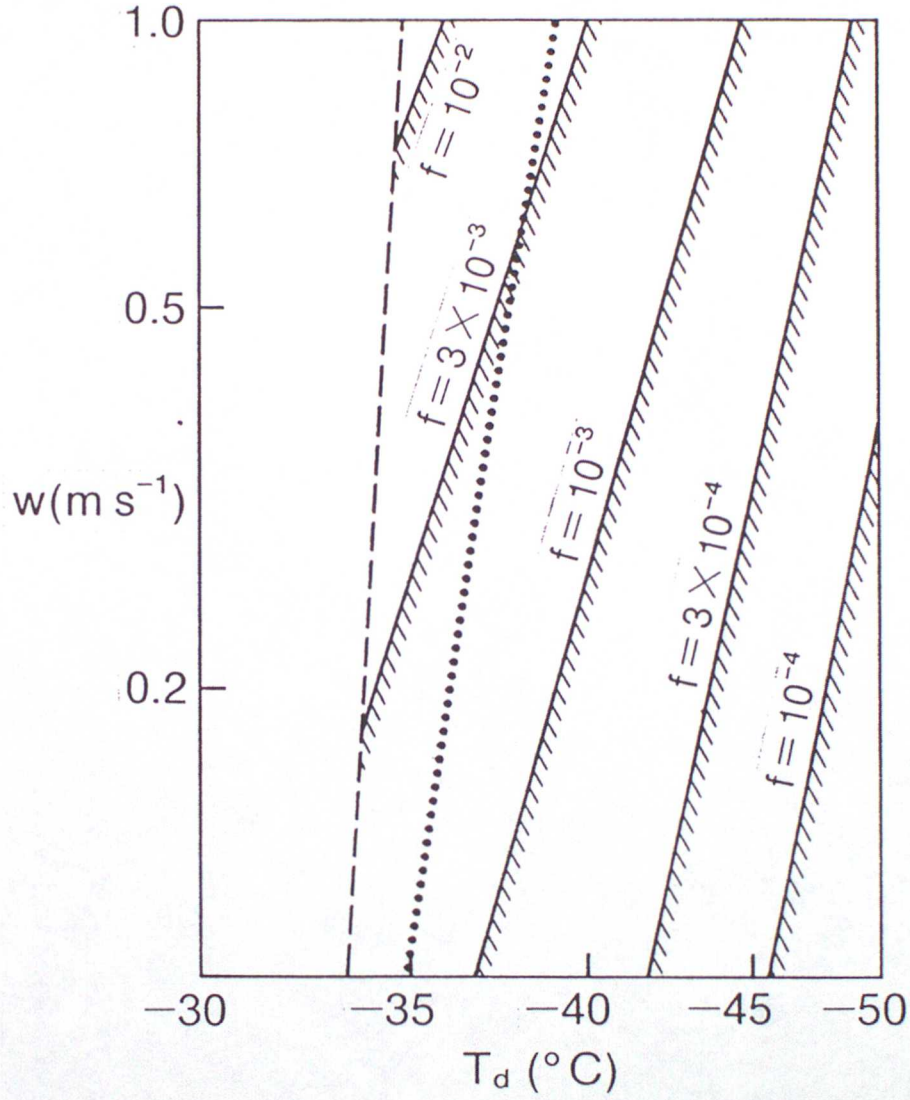

Table 1

VERTICAL VELOCITY ($m\ s^{-1}$)	DEW POINT −35° C	DEW POINT −50° C
0.1	$r = 60\ \mu m$ $\tau = 600$ sec	$r = 39\ \mu m$ $\tau = 400$ sec
1.0	$r = 17\ \mu m$ $\tau = 55$ sec	$r = 11\ \mu m$ $\tau = 20$ sec

Table 1 Average radii, r, of initial ice crystals nucleated homogeneously and the timescale τ, of the freezing process.

Dawson QJ Table 2

Table 2

VERTICAL VELOCITY ($m\ s^{-1}$)	DEW POINT −35° C	DEW POINT −50° C
0.1	r = 70 μm τ = 1250 sec	r = 40 μm τ = 1000 sec
1.0	r = 30 μm τ = 200 sec	r = 15 μm τ = 100 sec

Table 2. Average radii, r, of initial ice crystals nucleated by deposition and the timescale τ, of the freezing process.

Table 3

Nucleation mode	A	α	β
Homogeneous	4.6×10^{-3}	39.1	0.05
Condensation–freezing	3.6×10^{-3}	33.2	0.07
Deposition	8.0×10^{-3}	29.0	0.09

Table 4

Lifetime τ_f of cloud containing 0.5×10^{-4} kg m^{-3} liquid water, with respect to homogeneous freezing, at various temperatures T_c. It is assumed 10^6 m^{-3} crystals form.

T_c	τ_f (sec)
−37	0.115
−36	1.17
−35	14.0
−34	207.0
−33	3.95×10^3

Table 5

Lifetime τ_f of cloud containing 0.5×10^{-4} kg m^{-3} liquid water, with respect to homogeneous nucleation, at various temperatures T_c. The Fletcher distribution of ice nuclei is assumed.

T_c	τ_f (sec)
−36	6.0
−32	31.0
−28	152.0
−24	757.0
−20	3.77×10^3

APPENDIX 3. HOW TO RUN THE CIRRUS MICROPHYSICS MODEL.

The source code resides in M15.SRCELIB(MCIMM).

A load module is in M15.LOADLIB(MCIMM)

The JCL for creating this is in M15.MMJCL.CNTL(LOAD)

The JCL for running the model is in M15.MMJCL.CNTL(MCIMM)

A 3.1 INPUTS

The input stream, which is read by subroutine INPUT, is as follows:

Variable	Format
IDENT	A30
IHOM, IHOTYP, IHOSUP	*
IDEP, IDETYP	*
ICONFR, ICOTYP	*
DT	*
NCCN	I2
NIBINS	I2
RD(1), ANDR(1)	2(E8.2,1X)
: :	
RD(NCCN), ANDR(NCCN)	
RC(1), ANCR(1)	2(E8.2,1X)

:	:
RC(NIBINS),ANCR(NIBINS)	
TD	E8.2
VERT	E8.2
HEIGHT	E8.2
ICON	I2

These variables have the following meanings:

IDENT: A run ID which appears on plotted O/P.

IHOM: Must have the value 0 or 1 (homogneous freezing 'switched off' or 'switched on')

IHOTYP: Must have the value 1 or 2. Usually IHOTYP=1. If IHOTYP = 2 is used the above value for Φ_{SL} (which is stored in common /PARM2/ is overwritten with $\Phi_{SL} = 2.1 \times 10^{-2} Nm^{-1}$ and the Pruppacher and Klett (1978) formula for Φ_{SL} is used. This facility is to test the model sensitivity to these quantities.

IHOSUP: Must have the value 1 or 2. The model is usually run with IHOSUP =1. If IHOSUP = 2 then DELGS calculates solute suppression with double the correct Van't Hoft factor (to test sensitivity to this).

IDEP: Must have the value 0 or 1 (deposition nucleation 'switched off' or on)

IDETYP: Selects one of three deposition nucleation models:

IDETYP = 1: $v(T) = 10^{-2}\exp(-0.6T)$

IDETYP = 2: $v(T) = 2.2\times10^{-1}\exp(-0.45T)$

IDETYP = 3: $v(T) = 2.7\times10^{10}\sigma_s^{10.6}$

The results in the above paper were obtained using (1). The depletion factor must be introduced by editing subroutine DEPFRZ.

ICONFR: Must be set to 0 or 1 (condensation-freezing off or on)

ICOTYP: Set to 1 at present (as only one c-f model in use)

DT: Numerical timestep. DT=0.5 usually adequate to achieve satisfactory results.

NCCN: The number of nucleus/droplet size bins in the model. Must be in the range 1 to 10 inclusive.

NIBINS: The number of crystal size bins, in range 9+NCCN to 26 inclusive.

RD(I),ANDR(I): Radii (m) and number concentration (m^{-3}) (ie total number in bin) of dry nuclei at start of run.

RC(I),ANCR(I): Radii (m) and number concentrations (m^{-3}) of any ice crystals present. There should be NIBINS entries even if there are no crystals at the start of the run, when ANCR(I) = 0.0. Any non zero entries for ANCR should be placed at the end of the list.

TD: Parcel dew point (deg C)

VERT: Parcel vertical velocity (ms^{-1})

HEIGHT: Height (m) above the condensation level to which integration will proceed.

ICON: =1, or 2. If there is a conflict between conservation of total water and total particle number ICON determines the priority IICON = 1 for water, ICON = 2 for number). Normally they are both conserved and ICON is unimportant.

A 3.2 RUNTIME

A rough guide is 0.05 CPU seconds (approx 0.025 units) per numerical step on the IBM 3081, although this depends on the initial conditions and which nucleation types are included. The number of steps is easily calculated from the total ascent of the parcel, the vertical velocity and DT. The ascent is approximately HEIGHT + 500.

A 3.3 OUTPUT

i) Line printer

Prints a summary table of various parameters output at 10 metre intervals. These are:

STEP NMBR: step number (also appears on plotter and fiche o/p). NB this number refers to output point, not numerical step.

ASCENT: height above starting level (m)

TEMP(PARCEL): parcel temp (deg C) (includes latent heat, although this is usually small).

CLOUD BINS: the number of size bins containing active cloud droplets.

CLOUD CONC: the total number of droplets contained in these bins (m^{-3}).

LWC: liquid water content (kgm^{-3}) (= total liquid water in droplets, including haze, minus liquid water contained in haze droplets active at start of run).

SIGW: water super-saturation (expressed as ratio, not %)

DROP LINR MEAN RAD: mean radius of active cloud droplets.

DROP MASS MEAN RAD: mass-weighted mean active droplet radius.

CRYSTAL CONC: concentration of ice crystals (m^{-3})

IWC: ice water content (kgm^{-3})

SIGI: ice super-saturation ratio (expressed as ratio, not %)

CRYST LINR MEAN RAD: mean ice crystal radius.

CRYST MASS MEAN RAD: mass-weighted mean crystal radius

Following the table is:

a) a summary of the total number of ice crystals nucleated by different mechanisims.

b) dry, moist, and frosty adiabatic lapse rates at the condensation level.

c) growthate coefficients for droplets and ice crystals ($m^2 s^{-1}$)

ii) Plotter

Plotted O/P comprises:

a) Log differential spectra of haze/cloud droplets, and ice crystals. Approximately 6 sets of these are produced, spanning the period when nucleation is in progress.

Plots of the following as functions of height above starting level:

b) Temperature of parcel

c) Cooling rate of parcel

d) Concentration of active cloud droplets

e) Ice crystal concentration

f) Liquid water content

g) Ice water content

h) Ice and water saturation ratios

i) Radii of each of the NCCN droplet size bins in the model.

iii) Fiche

a) Subroutine INPUT prints a verification of the inputs described above, after the message 'SUBROUTINE INPUT CALLED'

b) Subroutine START calculates the starting conditions for the integration from the inputs. The parcel is assumed to start its ascent from the frost point. The corresponding altitude and pressure are calculated assuming a NACA standard atmosphere. A condensation level is calculated assuming adiabatic ascent. This information, together with the total initial number of CCN, the total initial number of ice crystals and the dry nucleus masses, is printed after the message 'SUBROUTINE START CALLED'.

c) Subroutine INIT calculates the starting values of variables appearing in the argument list of the differential equation solver DES2. X and XEND are the initial and final altitudes. The integration is performed in sub-intervals of length XINT (set internally: it may be altered by changing the appropriate line of subroutine INIT). N is the number of variables in the equation set. TOL is a tolerance value (again set internally, but easily altered by

changing the code.) INIT also sets the radii of any dry nuclei which are activated to haze droplets at starting humidity. These variables are all printed after the message 'SUBROUTINE INIT CALLED'.

d) The differential equation solver DES2 is then called INT((XEND=X)/XINT) times, once for each sub-interval, printing the message 'CALL TO DES2 (number)' Various errors and warnings may appear during execution, the most common of which are:

'NO CONVERGENCE IN DES2, AMAX=.....' This warning indicates that for at least one of the variables in the equation set the fractional (or absolute if y <1.) error in the new estimate of y has failed to fall below the value TOL in the maximum number of iterations allowed. This warning is quite common, particularly when cloud condensation of freezing are occuring. If AMAX achieves values comparable to 1. the model should be re run with a smaller timestep.

'WARNING: TOO FEW ICE BINS, RCMIN=...' warns that by the end of the next integration sub-intervalthe smallest ice bins will have become active and reached a radius RCMIN. This may be larger than some, or all, of the droplet size bins, preventing conservation of mass and number, as described above. This only occurs at low updraught. It rarely has serious consequences, but conservation should be checked.

'SUBROUTINE GROW1: DAMPING SWITCHED ON, DROP NUMBER.....'
'SUBROUTINE GROW1: DAMPING SWITCHED OFF, DROP NUMBER.....'
indicate the damping of droplet growth. When condensation occurs all

active cloud drops should be un-damped. Damping is re-introduced when evaporation occurs.

'GROW1: DAMPING FOR EVAPORATION APPLIED'. When the saturation ratio is falling rapidly the shrinking droplets are damped with an exponential time constant of 2.*DT to avoid numerical instability (eg negative radii). The effects of this on the solutions may be assessed by running the model with various steplengths.

'FREEZ: DAMPING FOR FREEZING APPLIED'

'CONFRZ: DAMPING FOR FREEZING APPLIED'

For rapid freezing, the rate of decrease of number in any one droplet bin is damped with a exponential time constant of 4.*DT to prevent instabbility (eg negative number concentrations). The effects of this on the solutions may be assessed by running the model with various steplengths.

'CONVERGENCE FAILURE IN ACTIV3' warns that the Newton-Raphson method for calculating equilibrium haze droplet radius has failed. The value at the last iteration is used. This appears to have no adverse side-effects.

Other error messages may be produced if DT is too large. These always bear the name of the relevant subroutine.

Occasionally subroutine DMIX generates underflow errors. These are of no consequence.

e) One the integration is complete a call to subroutine OUTPUT is signalled, followed by some notes and frequently the warning message 'WARNING: IODMP=0 ON COMPLETION OF RUN'. This merely signifies that at least one droplet bin has not become activated to a cloud droplet during the run. Then follow a number of pages of O/P, one for each integration sub-interval. The header of each page contains the following:

STEP NO: sub-interval number

TIME: time

HEIGHT: height above MSL (NACA)

ASCENT " " starting point

PRESS(DA)

RHO(DA) atmospheric state (from starting state, assuming DALR)

TEMP(DALR)

TEMP(PARCEL): parcel temperature, allowing for latent heat.

SIGW water saturation ratio

SIGI ice saturation ratio

ABS HUM absolute humidity

Then follow details of the droplet spectrum. The variables IACTIV and ICLDO indicate activated haze drops (as opposed to dry nuclei) and actively growing cloud drops, respectively. The remainder of the O/P is self explanatory.

f) Finally, subroutine PLT generates a message indicating successful

plotting.

A 3.4 FUTURE MODIFICATIONS

i) Homogeneous freezing. If new information on the classical theory of homogeneous nucleation becomes available and its effects need to be modelled than allow additional values of IHOTYP and IHOSUP and add appropriate sections to subroutine DELG and DELGS.

ii) Deposition nucleation. Additional models may be introduced by allowing further values of IDETYP and introducing appropriate sections in DEPFRZ.

iii) Condensation-freezing. Only one model is available at present. New models may be introduced by allowing further values of ICOTYP and adding corresponding code to subroutine CONFRZ.